行政院國家科學委員會專題研究計畫 成果報告

由強場雷射所驅動的相對論性電子運動（IV）
研究成果報告(精簡版)

計 畫 類 別 ：個別型
計 畫 編 號 ：NSC 99-2115-M-029-002-
執 行 期 間 ：99 年 08 月 01 日至 100 年 10 月 31 日
執 行 單 位 ：東海大學數學系

計 畫 主 持 人：曹景懿
共 同 主 持 人：汪治平
計畫參與人員：其他-兼任助理人員：康迺豪

報 告 附 件 ：出席國際會議研究心得報告及發表論文

處 理 方 式 ：本計畫可公開查詢

中 華 民 國 100 年 10 月 06 日

Relativistic birefringence induced by a high-intensity laser field in a plasma

G. Tsaur,[1] N.-H. Kang,[2] Z.-H. Xie,[3] S.-H. Chen,[4] and J. Wang[3,4,5]
[1]*Department of Mathematics, Tunghai University, Taichung 40704, Taiwan*
[2]*Department of Physics, National Tsing Hua University, Hsinchu 30013, Taiwan*
[3]*Department of Physics, National Taiwan University, Taipei 10617, Taiwan*
[4]*Department of Physics, National Central University, Jhongli 32001, Taiwan*
[5]*Institute of Atomic and Molecular Sciences, Academia Sinica, Taipei 10617, Taiwan*
(Received 20 September 2010; published 2 March 2011)

Field-induced birefringence, also known as cross-polarization wave generation, has played an important role in ultrafast nonlinear optics. In this paper we analyze birefringence induced by relativistic collective motion of electrons driven by a high-intensity laser field. An analytical expression for the phase difference between the parallel and perpendicular polarizations of a weak probe pulse with respect to the polarization of a strong pump pulse as a function of intensity, density, and wavelengths is derived. It is shown that under typical experimental conditions of high-field physics, the effect is well above detection threshold. The analysis is compared with particle-in-cell simulations, and the agreement provides good support for the theory.

DOI: 10.1103/PhysRevA.83.033801 PACS number(s): 42.65.Re, 52.38.−r, 42.25.Lc

I. INTRODUCTION

Relativistic nonlinear optics is a research field recently emerged from the rapid development of high-intensity lasers [1]. In relativistic nonlinear optics the field in the laser pulse is much stronger than the field that binds the outer electrons of atoms and molecules, to the extent that the $\mathbf{v} \times \mathbf{B}$ term in the Lorentz force cannot be ignored. As a result the nonlinearity comes from the relativistic motion of free electrons instead of the anharmonicity of the bound-electron oscillation in atoms and molecules. Terawatt-class lasers have been utilized to induce relativistic nonlinear optical phenomena in underdense plasmas, including harmonic generation [2–4], self-focusing [5–7], self-phase-modulation [8], pulse compression [9], and optical rectification [10,11]. These phenomena have also been studied by theoretical analysis [12–21] and computer simulation [22–28].

Field-induced birefringence, also known as cross-polarization wave generation, has played an important role in ultrafast nonlinear optics. It is utilized in fiber mode-locking lasers to generate femtosecond laser pulses [29,30]. It is the key element of frequency-resolved optical-gating—the first method capable of reconstructing the femtosecond laser wave form (both amplitude and phase profiles) [31]. It is the mechanism underlying the most effective method for enhancing the contrast of femtosecond high-intensity lasers [32]. It has also been used to image the propagation dynamics of intense light in a medium [33]. In the extreme case, experimental observation of vacuum birefringence induced by virtual electron-position pair creation has been considered [34].

In this paper we study relativistic birefringence induced by a strong propagating laser field in underdense plasmas. For relativistic nonlinear optics it is natural to consider a fully ionized plasma as the nonlinear medium. This is because plasma will not be damaged by a high-intensity laser, and plasma is not limited by absorption in the deep uv spectral range and beyond. In addition, transient plasma structures can be fabricated by synchronized laser pulses to enhance the nonlinear interaction [4]. We analyze the relativistic motion of plasma electrons driven by a strong linearly polarized pump beam and a weak probe beam polarized at 45° with respect to the polarization axis of the pump beam. Because of the nonlinear relativistic motion of the electrons, the probe beam experiences different indices of refraction in its two polarization axes, and this results in a phase difference between the two polarizations as a function of the intensity of the pump beam, the plasma density, and the wavelengths of the pump and probe beams. This makes the medium birefringent for the probe beam.

In relativistic nonlinear optics, a relevant parameter is the amplitude a of the normalized vector potential. Relativistic effects become significant when a is not much smaller than 1. Although relativistic nonlinear effects can be analyzed by using a as the perturbation parameter, such an approach is valid only when $a \ll 1$. This is too restrictive considering that currently a tabletop multiterawatt laser can easily produce a field of $a > 1$. In this paper we use a'/a and $1 - \eta^2$ as the perturbation parameters to derive the first-order analytical solution that describes the relativistic birefringence induced by a laser beam, where a and a' are the amplitudes of the pump beam and probe beam, respectively, and η is the index of refraction. The starting point (unperturbed solution) is the fully relativistic solution for the case with $a' = 0$ and $\eta = 1$, which is exact for arbitrary a [15]. For most experiments $1 - \eta^2$ is on the order of 10^{-2} and a'/a can be chosen $\ll 1$; hence the first-order terms in the expansion already provide a useful approximate solution without being limited to $a \ll 1$. For field-induced birefringence it is not necessary to carry out a three-dimensional analysis. This is because in general third-order relativistic nonlinear effects do not rely on the transverse gradient of the driving field or the transverse gradient of the electron density, in contrast to second-harmonic generation and optical rectification [20,21].

In Sec. II the nonlinear equations of motion for the electrons driven by a high-intensity pump beam and a low-intensity probe beam are derived. In Sec. III first-order analytical solutions for the electron motion are derived. In Sec. IV the difference between the indices of refraction for the two polarization axes is derived as a function of the amplitude a,

the plasma density n_0, and the wave numbers k,k' of the pump and probe beams. Comparison with particle-in-cell simulations is carried out in Sec. V. The close agreement between the analytical calculation and simulation provides a good support for the theoretical analysis.

II. EQUATIONS OF MOTION FOR THE ELECTRONS

In the following analysis we assume the laser to be focused onto a preionized gas target. Preionization is done by the front edge of the laser pulse or by a prepulse that has a broader spatial profile and passes through the gas before the pump pulse [4]. The ions are too heavy to move significantly within the time scale of the laser pulse; hence they are considered as a static distribution of background positive charges. Since in the relativistic regime the energy of electrons' thermal motion is much smaller than that of their collectively driven motion, it is possible to ignore the thermal motion and assume that within the ultrashort time scale of the laser pulse the collectively driven motion can be described by a cold fluid model. To simplify the notation, in most places we use the normalized vector potential $\mathbf{a}$ and the normalized scalar potential ϕ to represent the electromagnetic fields. These two dimensionless quantities are defined by

$$\mathbf{a} \equiv \frac{|e|\mathbf{A}}{m_e c^2}, \quad \phi \equiv \frac{|e|\Phi}{m_e c^2}, \tag{2.1}$$

where $e = -|e|$ is the electron charge, m_e is the electron rest mass, c is the speed of light, $\mathbf{A}$ is the vector potential, and Φ is the scalar potential.

The pump and probe beams are both linearly polarized and propagating in the $\hat{z}$ direction. In a one-dimensional model the normalized vector potential of the pump beam is $a\sin(k\zeta)\,\hat{x}$ and that of the probe beam is $(a'/\sqrt{2})\sin(k'\zeta')(\hat{x}+\hat{y})$, where

$$\zeta = \eta z - ct, \quad \zeta' = \eta' z - ct, \tag{2.2}$$

and η, η' are the refractive indices of the pump and probe beams, respectively. In combination, the normalized vector potential $\mathbf{a} = a_1\hat{x} + a_2\hat{y} + a_3\hat{z}$ is

$$a_1 = a\sin(k\zeta) + \frac{a'}{\sqrt{2}}\sin(k'\zeta'), \tag{2.3}$$

$$a_2 = \frac{a'}{\sqrt{2}}\sin(k'\zeta'), \tag{2.4}$$

$$a_3 = 0. \tag{2.5}$$

We assume that the amplitudes $a(\zeta)$,$a'(\zeta')$ satisfy $a' \ll a$ and the slowly varying condition

$$\frac{da}{d\zeta} = O(k\epsilon a), \quad \frac{da'}{d\zeta'} = O(k'\epsilon a'), \tag{2.6}$$

where $\epsilon \ll 1$. We also assume that η,η' satisfy the condition of rarefied plasma

$$1-\eta^2 = O(\epsilon), \quad 1-\eta'^2 = O(\epsilon). \tag{2.7}$$

In the following analysis terms much smaller than $O(\epsilon)$ are ignored.

The analysis starts from the Lorentz equation $d\mathbf{p}/dt = e(\mathbf{E} + \mathbf{v}/c \times \mathbf{B})$ and the energy equation $d(m_e c^2\gamma)/dt = e\mathbf{v}\cdot\mathbf{E}$. They are equivalent to

$$\frac{d\mathbf{p}}{dt} = m_e c^2\left[\frac{1}{c}\frac{\partial \mathbf{a}}{\partial t} + \nabla\phi - \boldsymbol{\beta}\times(\nabla\times\mathbf{a})\right], \tag{2.8}$$

$$\frac{d}{dt}(m_e c\gamma) = m_e c^2\boldsymbol{\beta}\cdot\left(\frac{1}{c}\frac{\partial \mathbf{a}}{\partial t} + \nabla\phi\right), \tag{2.9}$$

where $\boldsymbol{\beta} = \mathbf{v}/c$. The normalized scalar potential satisfies the Poisson equation

$$\nabla^2\phi = k_p^2\left(\frac{n_e}{n_0} - 1\right), \tag{2.10}$$

where $k_p = \omega_p/c$ and $\omega_p = (4\pi e^2 n_0/m_e)^{1/2}$ is the plasma frequency for the ambient plasma density n_0, and n_e is the electron density. The quantities n_e and $\boldsymbol{\beta}$ are related by the continuity equation

$$\frac{\partial n_e}{\partial t} + c\nabla\cdot(n_e\boldsymbol{\beta}) = 0. \tag{2.11}$$

Using the notations $x_1 = x$, $x_2 = y$, $x_3 = z$, $x_4 = ct$, $\beta_4 = dx_4/(cdt) = 1$, and $a_4 = -\phi$, Eqs. (2.8) and (2.9) can be written as

$$\frac{dp_\mu}{dt} = m_e c^2\sum_{\nu=1}^{4}\beta_\nu\left(\frac{\partial a_\mu}{\partial x_\nu} - \frac{\partial a_\nu}{\partial x_\mu}\right), \tag{2.12}$$

$$\frac{d}{dt}(m_e c\gamma) = m_e c^2\sum_{\nu=1}^{4}\beta_\nu\left(\frac{\partial a_\nu}{\partial x_4} - \frac{\partial a_4}{\partial x_\nu}\right). \tag{2.13}$$

Using the same notations, $(d/dt)\,a_\mu = (\partial/\partial t + c\boldsymbol{\beta}\cdot\nabla)\,a_\mu$ can be written as

$$\frac{da_\mu}{dt} = c\sum_{\nu=1}^{4}\beta_\nu\frac{\partial a_\mu}{\partial x_\nu}; \tag{2.14}$$

hence the first term in the right-hand side of Eq. (2.12) is $m_e c(da_\mu/dt)$ and the second term in the right-hand side of Eq. (2.13) is $-m_e c(da_4/dt) = m_e c(d\phi/dt)$. Therefore Eqs. (2.12) and (2.13) are equivalent to

$$\frac{d}{dt}(p_\mu - m_e c a_\mu) = -m_e c^2\sum_{\nu=1}^{4}\beta_\nu\frac{\partial a_\nu}{\partial x_\mu}, \tag{2.15}$$

$$\frac{d}{dt}m_e c\,(\gamma - \phi) = m_e c^2\sum_{\nu=1}^{4}\beta_\nu\frac{\partial a_\nu}{\partial x_4}. \tag{2.16}$$

For $\mu = 1$ or 2, one may write Eq. (2.15) as

$$\frac{d}{dt}\,(p_\perp - m_e c a_\perp) = -m_e c^2\sum_{\nu=1}^{4}\beta_\nu\frac{\partial a_\nu}{\partial x_\perp}. \tag{2.17}$$

For $\mu = 3$, since $a_3 = 0$, one may write Eq. (2.15) as

$$\frac{dp_\parallel}{dt} = -m_e c^2\sum_{\nu=1,2,4}\beta_\nu\frac{\partial a_\nu}{\partial x_\parallel}. \tag{2.18}$$

Subtracting η times Eq. (2.16) from Eq. (2.18), one obtains

$$\frac{d}{dt}[p_\parallel - m_e c\eta(\gamma-\phi)] = -m_e c^2 \sum_{\nu=1,2,4} \beta_\nu \left(\frac{\partial}{\partial x_\parallel} + \frac{\eta}{c}\frac{\partial}{\partial t}\right) a_\nu. \tag{2.19}$$

The subscript $\perp$ represents the x and y components, and the subscript $\parallel$ represents the z component. Because a_ν do not depend on $x_\perp$, the right-hand side of Eq. (2.17) is zero. Define $f_\parallel$ such that the right-hand side of Eq. (2.19) is equal to $d(m_e c\eta f_\parallel)/dt$, namely,

$$\frac{d}{dt}(m_e c\eta f_\parallel) \equiv -m_e c^2 \sum_{\nu=1,2,4} \beta_\nu \left(\frac{\partial}{\partial x_\parallel} + \frac{\eta}{c}\frac{\partial}{\partial t}\right) a_\nu. \tag{2.20}$$

Then Eqs. (2.17) and (2.19) become

$$\frac{d}{dt}(p_\perp - m_e c a_\perp) = 0, \tag{2.21}$$

$$\frac{d}{dt}[p_\parallel - m_e c\eta(\gamma-\phi)] = \frac{d}{dt}(m_e c\eta f_\parallel). \tag{2.22}$$

The solutions are

$$p_\perp = m_e c a_\perp, \tag{2.23}$$

$$p_\parallel = m_e c\eta(\gamma - 1 - \phi + f_\parallel). \tag{2.24}$$

The integration constant -1 is added after γ in Eq. (2.24) such that the initial condition $p_\perp = p_\parallel = 0$ is satisfied when $a = a' = 0$. From $\boldsymbol{\beta} = \mathbf{p}/(m_e c\gamma)$ one has

$$\beta_\perp = \frac{a_\perp}{\gamma}, \tag{2.25}$$

$$\beta_\parallel = \eta - \frac{\eta(1+\phi-f_\parallel)}{\gamma}. \tag{2.26}$$

Moreover, from $\gamma^2(1-\beta_\perp^2-\beta_\parallel^2)=1$ one obtains $(1-\eta^2)\gamma^2 + 2B\gamma - C = 0$, where $B = \eta^2(1+\phi-f_\parallel)$ and $C = 1 + a_\perp^2 + \eta^2(1+\phi-f_\parallel)^2$. Therefore to the first order of $1-\eta^2$ one has $\gamma = C/(2B) - (1-\eta^2)C^2/(8B^3)$, namely,

$$\gamma = \frac{1 + a_\perp^2 + \eta^2(1+\phi-f_\parallel)^2}{2\eta^2(1+\phi-f_\parallel)} - (1-\eta^2)\frac{[1 + a_\perp^2 + \eta^2(1+\phi-f_\parallel)^2]^2}{8\eta^6(1+\phi-f_\parallel)^3}, \tag{2.27}$$

where ϕ and n_e are determined by Eqs. (2.10) and (2.11), and $f_\parallel$ by Eq. (2.20). Because $[\partial/\partial x_\parallel + (\eta/c)(\partial/\partial t)]\zeta = 0$, in Eq. (2.20) only the derivative of the probe beam with the phase $k'\zeta'$ and the amplitude $a'(\zeta')$ is nonzero. That is, $f_\parallel = 0$ if $a' = 0$. When $f_\parallel = 0$ and $\eta = 1$, Eqs. (2.23)–(2.27) reduce to the solutions in Ref. [15]. In Sec. III ϕ, n_e, and $f_\parallel$ will be solved and in Sec. IV the solutions will be used to evaluate the difference between the refractive indices for the two polarization axes experienced by the probe beam.

III. THE SOLUTIONS

In this section we complete the solutions in Eqs. (2.23)–(2.27) by solving for ϕ and n_e from Eqs. (2.10) and (2.11), and for $f_\parallel$ from Eq. (2.20). Set $\phi = \phi_s + \phi_f$, where ϕ_s is the slowly varying part of ϕ and ϕ_f is the fast-varying part. As we shall see in Sec. III A $\phi_f \ll \phi_s$, and $\phi_s = O(a)$ when the amplitude a is not much smaller than 1. Moreover, as we shall see in Sec. IV, the refractive indices satisfy

$$1-\eta^2 = \frac{k_p^2/k^2}{1+\phi_s}, \quad 1-\eta'^2 = \frac{k_p^2/k'^2}{1+\phi_s}; \tag{3.1}$$

hence the assumption in Eq. (2.7) is equivalent to

$$\frac{k_p^2}{k^2} = O(\epsilon a), \quad \frac{k_p^2}{k'^2} = O(\epsilon a). \tag{3.2}$$

In Secs. III, IV, and V we consider the case with $|k-k'| = O(k)$ and in Sec. VI the case with $|k-k'| \ll k$ is discussed.

A. Solution of ϕ

In order to solve for ϕ from Eq. (2.10), one needs to evaluate n_e/n_0 first. For the case with $a' = 0$ and $\eta = 1$, the solution of n_e/n_0 is [15]

$$\frac{n_e}{n_0} = \frac{\gamma}{1+\phi}. \tag{3.3}$$

We can make an educated guess that the lowest-order approximation for n_e/n_0 is still of the same form for the case with $a' \ll a$ and $1-\eta^2 = O(\epsilon)$. This guess will be verified in Sec. III C. Therefore to the lowest order, Eq. (2.10) is equivalent to

$$\nabla^2\phi = k_p^2\left(\frac{\gamma}{1+\phi} - 1\right). \tag{3.4}$$

Keeping only the lowest-order terms in Eq. (2.27), namely, neglecting $f_\parallel$,ϕ_f and setting $\eta = 1$, one obtains

$$\gamma \approx \frac{1+a_\perp^2}{2(1+\phi_s)} + \frac{1+\phi_s}{2} \tag{3.5}$$

and

$$\frac{\gamma}{1+\phi} - 1 \approx \frac{\gamma}{1+\phi_s} - 1 \approx \frac{1+a_\perp^2}{2(1+\phi_s)^2} - \frac{1}{2}. \tag{3.6}$$

From Eqs. (2.3) and (2.4) one has, by neglecting the terms with a'^2,

$$a_\perp^2 = a_1^2 + a_2^2 \approx \frac{a^2}{2}[1-\cos(2k\zeta)] - \frac{aa'}{\sqrt{2}}(\cos\theta_+ - \cos\theta_-), \tag{3.7}$$

where $\theta_\pm \equiv k\zeta \pm k'\zeta'$. Therefore Eq. (3.4) can be separated into the slowly and fast-varying parts as follows:

$$\nabla^2\phi_s = k_p^2\left[\frac{1+a^2/2}{2(1+\phi_s)^2} - \frac{1}{2}\right], \tag{3.8}$$

$$\nabla^2\phi_f = \frac{-k_p^2}{2(1+\phi_s)^2}\left[\frac{a^2}{2}\cos(2k\zeta) + \frac{aa'}{\sqrt{2}}(\cos\theta_+ - \cos\theta_-)\right]. \tag{3.9}$$

Note that the term $\cos\theta_- = \cos(k\zeta - k'\zeta')$ belongs to the fast-varying part, because here $|k-k'| = O(k)$ is assumed. Equation (3.8) leads to

$$(1+\phi_s)^2 = \frac{1+a^2/2}{1+2\nabla^2\phi_s/k_p^2}. \tag{3.10}$$

If $\nabla^2\phi_s \ll k_p^2$, Eq. (3.10) becomes approximately

$$(1+\phi_s)^2 = 1+\frac{a^2}{2}, \tag{3.11}$$

namely,

$$\phi_s = \sqrt{1+\frac{a^2}{2}} - 1, \tag{3.12}$$

which implies $\phi_s = O(a)$ when a is not much smaller than 1. The condition $\nabla^2\phi_s \ll k_p^2$ holds, because Eqs. (2.6) and (3.2) imply $\nabla^2\phi_s = \mathrm{O}(k^2\epsilon^2 a) = \mathrm{O}(k_p^2\epsilon)$. Since in the one-dimensional case ϕ_f does not depend on $x_\perp$, one has $\nabla^2\phi_f = \partial^2\phi_f/\partial x_\parallel^2$; hence Eqs. (3.9) and (3.11) imply approximately

$$\phi_f = \frac{k_p^2}{2(1+a^2/2)}\left[\frac{a^2}{8k^2}\cos(2k\zeta) + \frac{aa'}{\sqrt{2}}\left(\frac{\cos\theta_+}{k_+^2} - \frac{\cos\theta_-}{k_-^2}\right)\right], \tag{3.13}$$

where $\theta_\pm \equiv k\zeta \pm k'\zeta' \approx (k\pm k')(z-ct)$ and $k_\pm \equiv k \pm k' = O(k)$. Using Eq. (3.2) one can see that $\phi_f = O(\epsilon a)$ and consequently $\phi_f \ll \phi_s$. Equations (3.12) and (3.13) are the lowest-order solutions of ϕ_s and ϕ_f. Note that for ϕ_f the lowest order means $O(\epsilon a)$ for the $\cos(2k\zeta)$ term and $O(\epsilon a')$ for the $\cos\theta_\pm$ terms. Even though the $\cos\theta_\pm$ terms are much smaller than the $\cos(2k\zeta)$ term in Eq. (3.13), as we shall see in Sec. IV, only the $\cos\theta_\pm$ terms are relevant to the birefringent effect.

B. Solution of $f_\parallel$

The term $f_\parallel$ is defined in Eq. (2.20), which is equivalent to

$$\frac{d}{dt}(\eta f_\parallel) = -c\sum_{\nu=1,2,4}\beta_\nu\left(\frac{\partial}{\partial x_\parallel} + \frac{\eta}{c}\frac{\partial}{\partial t}\right)a_\nu. \tag{3.14}$$

Since $[\partial/\partial x_\parallel + (\eta/c)(\partial/\partial t)]\zeta = 0$, the derivative of $a_4 = -\phi$ equals the derivative of the $\cos\theta_\pm$ terms in Eq. (3.13) and the derivatives of a_1 and a_2 equal the derivatives of the $(a'/\sqrt{2})\sin(k'\zeta')$ terms in Eqs. (2.3) and (2.4). As mentioned at the end of Sec. III A, the terms with $\cos\theta_\pm$ in Eq. (3.13) are $O(\epsilon a')$, while the term $(a'/\sqrt{2})\sin(k'\zeta')$ in Eqs. (2.3) and (2.4) is $O(a')$; therefore to the lowest order the term with $\nu = 4$ in Eq. (3.14) can be neglected. Equation (3.14) is approximately

$$\frac{df_\parallel}{dt} = -c\sum_{\nu=1,2}\beta_\nu\left(\frac{\partial}{\partial x_\parallel} + \frac{\eta}{c}\frac{\partial}{\partial t}\right)a_\nu. \tag{3.15}$$

Since $\beta_\nu = a_\nu/\gamma$ for $\nu = 1,2$, Eq. (3.15) can be written as

$$\frac{df_\parallel}{dt} = -\frac{c}{2\gamma}\left(\frac{\partial}{\partial x_\parallel} + \frac{\eta}{c}\frac{\partial}{\partial t}\right)a_\perp^2, \tag{3.16}$$

where $a_\perp^2$ is given in Eq. (3.7). From Eq. (3.7) and $[\partial/\partial x_\parallel + (\eta/c)(\partial/\partial t)]\zeta = 0$, Eq. (3.16) equals

$$\frac{df_\parallel}{dt} = \frac{aa'}{2\sqrt{2}}\frac{c}{\gamma}\left(\frac{\partial}{\partial x_\parallel} + \frac{\eta}{c}\frac{\partial}{\partial t}\right)(\cos\theta_+ - \cos\theta_-). \tag{3.17}$$

Since $\theta_\pm \equiv k\zeta \pm k'\zeta'$, one has

$$\left(\frac{\partial}{\partial x_\parallel} + \frac{\eta}{c}\frac{\partial}{\partial t}\right)\theta_\pm = \pm k'(\eta'-\eta). \tag{3.18}$$

Moreover, the term $1/\gamma$ in the right-hand side of Eq. (3.17) can be changed to $d\theta_\pm/dt$ by using the following procedure. From $\zeta = \eta z - ct$ and Eq. (2.26) one obtains

$$\frac{d\zeta}{dt} \approx c(\beta_\parallel - 1) \approx -c\frac{1+\phi_s}{\gamma}. \tag{3.19}$$

From $\theta_\pm \approx k_\pm\zeta$ and Eq. (3.19), one gets

$$\frac{1}{\gamma} \approx \frac{-1}{ck_\pm(1+\phi_s)}\frac{d\theta_\pm}{dt}. \tag{3.20}$$

Set $\mathbf{D} = \partial/\partial x_\parallel + (\eta/c)(\partial/\partial t)$ and $F = F(\theta_i)$ with $i = +$ or $-$. The right-hand side of Eq. (3.17) contains terms of the form $(1/\gamma)\mathbf{D}F$. Because $\mathbf{D}F = C(dF/d\theta_i)$, where $C = \mathbf{D}\theta_i = \pm k'(\eta'-\eta)$ as shown in Eq. (3.18), and $1/\gamma \approx \tilde{C}(d\theta_i/dt)$, where $\tilde{C} = -1/[ck_\pm(1+\phi_s)]$ as shown in Eq. (3.20), one has

$$\frac{1}{\gamma}(\mathbf{D}F) \approx C\tilde{C}\frac{dF}{d\theta_i}\frac{d\theta_i}{dt} = C\tilde{C}\frac{dF}{dt}, \tag{3.21}$$

where $C\tilde{C} = k'(\eta-\eta')/[ck_+(1+\phi_s)]$ when $\theta_i = \theta_+$ and $C\tilde{C} = -k'(\eta-\eta')/[ck_-(1+\phi_s)]$ when $\theta_i = \theta_-$. Therefore, the right-hand side of Eq. (3.17) can be changed from $(1/\gamma)\mathbf{D}F$ to the form dF/dt as

$$\frac{df_\parallel}{dt} = \frac{aa'k'(\eta-\eta')}{2\sqrt{2}(1+\phi_s)}\frac{d}{dt}\left(\frac{\cos\theta_+}{k_+} + \frac{\cos\theta_-}{k_-}\right), \tag{3.22}$$

and the solution is approximately

$$f_\parallel = \frac{aa'k'(\eta-\eta')}{2\sqrt{2}(1+\phi_s)}\left(\frac{\cos\theta_+}{k_+} + \frac{\cos\theta_-}{k_-}\right). \tag{3.23}$$

From Eq. (3.1) and $k_\pm = k \pm k'$ one obtains

$$\eta - \eta' \approx \frac{-k_p^2}{2(1+\phi_s)}\left(\frac{1}{k^2} - \frac{1}{k'^2}\right) = \frac{k_p^2 k_+ k_-}{2(1+\phi_s)k^2k'^2}, \tag{3.24}$$

and Eq. (3.23) becomes

$$f_\parallel = \frac{k_p^2 aa'}{4\sqrt{2}(1+a^2/2)k^2k'}(k_-\cos\theta_+ + k_+\cos\theta_-). \tag{3.25}$$

Using Eq. (3.2) one can see that $f_\parallel = O(\epsilon a')$. This is the lowest-order solution of $f_\parallel$.

C. Solution of n_e

Finally we solve for n_e from Eq. (2.11). Equation (2.11) is equivalent to

$$\frac{\partial n_e}{\partial t} + c\boldsymbol{\beta}\cdot\nabla n_e + n_e c\nabla\cdot\boldsymbol{\beta} = 0. \tag{3.26}$$

Since $(\partial/\partial t + c\boldsymbol{\beta}\cdot\nabla)n_e = dn_e/dt$, Eq. (3.26) is equivalent to

$$\frac{dn_e}{dt} + n_e c\nabla\cdot\boldsymbol{\beta} = 0. \tag{3.27}$$

The solution is

$$n_e = n_0\exp\left(-\int c\nabla\cdot\boldsymbol{\beta}\,dt\right). \tag{3.28}$$

To obtain the value n_e/n_0, we must evaluate the integral in Eq. (3.28). Because $\nabla\cdot(\gamma\boldsymbol{\beta})$ is much simpler than $\nabla\cdot\boldsymbol{\beta}$, we separate the integrand into two terms,

$$c\nabla\cdot\boldsymbol{\beta} = c\left[\gamma\boldsymbol{\beta}\cdot\nabla\frac{1}{\gamma} + \frac{1}{\gamma}\nabla\cdot(\gamma\boldsymbol{\beta})\right]. \tag{3.29}$$

From $\nabla(1/\gamma) = -(1/\gamma^2)\nabla\gamma$, the first term in Eq. (3.29) is

$$c\gamma\boldsymbol{\beta}\cdot\nabla\frac{1}{\gamma} = -\frac{1}{\gamma}(c\boldsymbol{\beta}\cdot\nabla\gamma) = -\frac{1}{\gamma}\left(\frac{d\gamma}{dt} - \frac{\partial\gamma}{\partial t}\right). \quad (3.30)$$

From Eqs. (2.25) and (2.26), the second term in Eq. (3.29) is

$$\frac{c}{\gamma}\nabla\cdot(\gamma\boldsymbol{\beta}) = \frac{c}{\gamma}\left\{\frac{\partial a_\perp}{\partial x_\perp} + \frac{\partial}{\partial x_\parallel}[\eta(\gamma - 1 - \phi + f_\parallel)]\right\} \approx \frac{c\eta}{\gamma}\frac{\partial}{\partial x_\parallel}(\gamma - \phi + f_\parallel), \quad (3.31)$$

where $\partial a_\perp/\partial x_\perp = 0$, because $a_\perp$ does not depend on $x_\perp$, and η can be taken as a constant, because its derivative $\partial\eta/\partial x_\parallel = O(k\epsilon^2)$ [obtained from Eq. (3.1), $k_p^2/k^2 = O(\epsilon a)$, and $\partial\phi_s/\partial x_\parallel = O(k\epsilon a)$] can be neglected. Substituting Eqs. (3.30) and (3.31) into (3.29), it becomes

$$c\nabla\cdot\boldsymbol{\beta} = -\frac{1}{\gamma}\frac{d\gamma}{dt} + \frac{1-\eta^2}{\gamma}\frac{\partial\gamma}{\partial t} + \frac{c\eta}{\gamma}\left(\frac{\partial}{\partial x_\parallel} + \frac{\eta}{c}\frac{\partial}{\partial t}\right)\gamma - \frac{c\eta}{\gamma}\frac{\partial(\phi - f_\parallel)}{\partial x_\parallel}, \quad (3.32)$$

where we subtracted $(\eta^2/\gamma)(\partial\gamma/\partial t)$ in the second term and added it back in the third term. To obtain n_e/n_0 in Eq. (3.28), we must evaluate the integral $\int c\nabla\cdot\boldsymbol{\beta}\,dt$. The first term in Eq. (3.32), which is equivalent to $-d(\ln\gamma)/dt$, can obviously be integrated. The other terms in Eq. (3.32) are all of the form $(1/\gamma)(\mathbf{D}F)$, where $\mathbf{D}$ represents the differential operator $\partial/\partial t$, $\partial/\partial x_\parallel + (\eta/c)(\partial/\partial t)$, or $\partial/\partial x_\parallel$. As mentioned in Sec. III B, when $\mathbf{D} = \partial/\partial x_\parallel + (\eta/c)(\partial/\partial t)$ the term can be changed to the form dF/dt. We shall show in what follows that terms with $\mathbf{D} = \partial/\partial t$ and $\mathbf{D} = \partial/\partial x_\parallel$ can also be changed to the form dF/dt. Hence they all can be integrated. For this purpose we set $\theta_1 = k\zeta$, $\theta_2 = \theta_+$, $\theta_3 = \theta_-$, and $k_1 = k$, $k_2 = k_+$, $k_3 = k_-$. First we show that the second term in Eq. (3.32) is approximately equivalent to $[(1-\eta^2)/(1+\phi_s)](d\gamma/dt)$. Let $F = F(\theta_i)$ with $i = 1$, 2, or 3, since $\partial\theta_i/\partial t = -ck_i$, one has

$$\frac{\partial F}{\partial t} = \frac{dF}{d\theta_i}\frac{\partial\theta_i}{\partial t} = -ck_i\frac{dF}{d\theta_i}. \quad (3.33)$$

Similar to the derivation of Eq. (3.20), from Eq. (3.19) and $\theta_i \approx k_i\zeta$ one has

$$\frac{1}{\gamma} \approx \frac{-1}{ck_i(1+\phi_s)}\frac{d\theta_i}{dt}. \quad (3.34)$$

Combining Eqs. (3.33) and (3.34), one gets

$$\frac{1}{\gamma}\frac{\partial F}{\partial t} \approx \frac{1}{1+\phi_s}\frac{dF}{dt}. \quad (3.35)$$

As can be seen from Eqs. (3.5) and (3.7), γ consists of functions $F(\theta_i)$ with $i = 1$, 2, or 3; therefore by Eq. (3.35) the second term in Eq. (3.32) is

$$\frac{1-\eta^2}{\gamma}\frac{\partial\gamma}{\partial t} \approx \frac{1-\eta^2}{1+\phi_s}\frac{d\gamma}{dt}. \quad (3.36)$$

Next we show that the last term in Eq. (3.32) is approximately $[1/(1+\phi_s)]d(\phi - f_\parallel)/dt$. Let $F = F(\theta_i)$ with $i = 1$, 2, or 3; since $\partial\theta_i/\partial x_\parallel \approx k_i$, one has

$$\frac{\partial F}{\partial x_\parallel} = \frac{dF}{d\theta_i}\frac{\partial\theta_i}{\partial x_\parallel} \approx k_i\frac{dF}{d\theta_i}. \quad (3.37)$$

Combining Eqs. (3.34) and (3.37), one gets

$$\frac{1}{\gamma}\frac{\partial F}{\partial x_\parallel} \approx \frac{-1}{c(1+\phi_s)}\frac{dF}{dt}. \quad (3.38)$$

As can be seen from Eqs. (3.13) and (3.25), $\phi - f_\parallel$ consists of functions $F(\theta_i)$ with $i = 1$, 2, or 3; therefore by Eq. (3.38) the last term in Eq. (3.32) is

$$-\frac{c\eta}{\gamma}\frac{\partial(\phi - f_\parallel)}{\partial x_\parallel} \approx \frac{1}{1+\phi_s}\frac{d(\phi - f_\parallel)}{dt} \approx \frac{1}{1+\phi}\frac{d\phi}{dt} - \frac{1}{1+\phi_s}\frac{df_\parallel}{dt}, \quad (3.39)$$

where for the first term in Eq. (3.39) the denominator $1+\phi_s$ is replaced by $1+\phi$. This can be done, because $d\phi/dt$ is small (ϕ_s is slowly varying and ϕ_f is small) and terms of order smaller than $d\phi/dt$ can be neglected. Finally we show that the third term in Eq. (3.32) is approximately $-[1/(1+\phi_s)](df_\parallel/dt)$. The differential operator for the third term is $\mathbf{D} = \partial/\partial x_\parallel + (\eta/c)(\partial/\partial t)$, the same as that in the right-hand side of Eq. (3.16). The proof can be done by simply comparing the third term with Eq. (3.16). Since ϕ_s is a function of $a(\zeta)$, one has $[\partial/\partial x_\parallel + (\eta/c)(\partial/\partial t)]\phi_s = 0$; hence from Eq. (3.5) the third term in Eq. (3.32) is

$$\frac{c\eta}{\gamma}\left(\frac{\partial}{\partial x_\parallel} + \frac{\eta}{c}\frac{\partial}{\partial t}\right)\gamma \approx \frac{c}{\gamma}\left(\frac{\partial}{\partial x_\parallel} + \frac{\eta}{c}\frac{\partial}{\partial t}\right)\frac{a_\perp^2}{2(1+\phi_s)}. \quad (3.40)$$

Comparing Eq. (3.40) with (3.16), one gets

$$\frac{c\eta}{\gamma}\left(\frac{\partial}{\partial x_\parallel} + \frac{\eta}{c}\frac{\partial}{\partial t}\right)\gamma \approx -\frac{1}{1+\phi_s}\frac{df_\parallel}{dt}. \quad (3.41)$$

Substituting Eqs. (3.36), (3.39), and (3.41) into Eq. (3.32), it becomes approximately

$$c\nabla\cdot\boldsymbol{\beta} = -\frac{1}{\gamma}\frac{d\gamma}{dt} + \frac{1}{1+\phi}\frac{d\phi}{dt} - \frac{d}{dt}\left(\frac{2f_\parallel}{1+\phi_s}\right) + (1-\eta^2)\frac{d}{dt}\left(\frac{\gamma}{1+\phi_s}\right). \quad (3.42)$$

From Eqs. (3.28) and (3.42), one obtains

$$\frac{n_e}{n_0} = \exp[\ln\gamma - \ln(1+\phi) + g], \quad (3.43)$$

where

$$g = \frac{2f_\parallel}{1+\phi_s} - (1-\eta^2)\left(\frac{\gamma}{1+\phi_s} - 1\right). \quad (3.44)$$

An integration constant -1 is added after $\gamma/(1+\phi_s)$ in Eq. (3.44) such that $g = 0$ is satisfied when $a = a' = 0$. Equation (3.44) is the lowest-order solution of g, whose first term contains $f_\parallel = O(\epsilon a')$ and second term contains $1-\eta^2$. If $a' = 0$ and $\eta = 1$, then g is zero. From $f_\parallel$ in Eq. (3.25), $1-\eta^2$ in Eq. (3.1), and $\gamma/(1+\phi_s) - 1$ in Eqs. (3.6) and (3.7), one obtains

$$g = \frac{k_p^2}{2(1+a^2/2)^{3/2}}\left[\frac{a^2}{2k^2}\cos(2k\zeta) + \frac{aa'}{\sqrt{2}kk'}(\cos\theta_+ + \cos\theta_-)\right]. \quad (3.45)$$

Comparing with ϕ_f in Eq. (3.13), one can see that g is of the same order as $\phi_f/\sqrt{1+a^2/2}$, namely, $O(\epsilon)$ for the $\cos(2k\zeta)$term and $O(\epsilon a'/a)$ for the $\cos\theta_\pm$ terms. Because $g \ll 1$, Eq. (3.43) is approximately

$$\frac{n_e}{n_0} = \frac{\gamma}{1+\phi}(1+g). \tag{3.46}$$

As mentioned before it differs from Eq. (3.3) only by a first-order perturbation term g. At this point we have completed the solutions of $\beta_\perp$, $\beta_\parallel$, ϕ, and n_e/n_0 to the first-order correction. These solutions will be used in Sec. IV for the analysis of relativistic birefringence.

IV. RELATIVISTIC BIREFRINGENCE

The time-dependent electron density n_e, electron velocity $\boldsymbol{\beta}$, and potential function ϕ derived in Secs. II and III serve as the source terms of the Maxwell equation. These source terms result from the nonlinear oscillation of the electrons, from which the change of the refractive indices in the two perpendicular axes can be derived. In the Coulomb gauge $\boldsymbol{\nabla}\cdot\mathbf{a}=0$, the normalized transverse Maxwell equation is

$$\left(\nabla^2 - \frac{1}{c^2}\frac{\partial^2}{\partial t^2}\right)a_\perp = k_p^2\frac{n_e}{n_0}\beta_\perp + \frac{\partial}{\partial x_\perp}\left(\frac{1}{c}\frac{\partial\phi}{\partial t}\right). \tag{4.1}$$

Because ϕ does not depend on $x_\perp$, it is

$$\left(\nabla^2 - \frac{1}{c^2}\frac{\partial^2}{\partial t^2}\right)a_\perp = k_p^2\frac{n_e}{n_0}\beta_\perp. \tag{4.2}$$

Equations (2.25) and (3.46) imply

$$\frac{n_e}{n_0}\beta_\perp = \frac{a_\perp}{1+\phi}(1+g) \approx \frac{a_\perp}{1+\phi_s}\left(1+g-\frac{\phi_f}{1+\phi_s}\right), \tag{4.3}$$

where $1+\phi=(1+\phi_s)[1+\phi_f/(1+\phi_s)]$. As mentioned after Eq. (3.45), both g and $\phi_f/(1+\phi_s)$ are $O(\epsilon)$. In Eq. (4.3) the first term $a_\perp/(1+\phi_s)$ is the lowest-order term and the others are the first-order perturbations. The Maxwell equation for the lowest-order driving field is

$$\left(\nabla^2 - \frac{\partial^2}{c^2\partial t^2} - \frac{k_p^2}{1+\phi_s}\right)a_\perp^{(l)} = 0. \tag{4.4}$$

The solutions are given in Eqs. (2.3) and (2.4) with the refractive indices

$$\eta = \sqrt{1-\frac{k_p^2/k^2}{1+\phi_s}}, \quad \eta' = \sqrt{1-\frac{k_p^2/k'^2}{1+\phi_s}}, \tag{4.5}$$

as mentioned in the beginning of Sec. III. In this paper we focus on how the refractive index is changed by the first-order perturbations. From Eq. (4.3) it can be seen that to the first-order correction the Maxwell equation is

$$\left(\nabla^2 - \frac{1}{c^2}\frac{\partial^2}{\partial t^2} - \frac{k_p^2}{1+\phi_s}\right)a_\perp = \frac{k_p^2 a_\perp}{1+\phi_s}\left(g-\frac{\phi_f}{1+\phi_s}\right). \tag{4.6}$$

From ϕ_f in Eq. (3.13) and g in Eq. (3.45), one obtains

$$\begin{aligned}\frac{k_p^2}{1+\phi_s}&\left(g-\frac{\phi_f}{1+\phi_s}\right)\\ &= \frac{k_p^4 aa'}{2\sqrt{2}(1+a^2/2)^2}\left[\frac{3a\cos(2k\zeta)}{4\sqrt{2}a'k^2} + \left(\frac{1}{kk'}-\frac{1}{k_+^2}\right)\cos\theta_+\right.\\ &\quad\left.+\left(\frac{1}{kk'}+\frac{1}{k_-^2}\right)\cos\theta_-\right],\end{aligned} \tag{4.7}$$

where $\theta_\pm \equiv k\zeta \pm k'\zeta'$ and $k_\pm = k \pm k'$. Moreover, from the $a_\perp$ in Eqs. (2.3) and (2.4), one has $a_1 \approx a\sin(k\zeta)$ and $a_2 \approx 0$. Hence for $\perp=1$ the right-hand side of Eq. (4.6) is approximately

$$\frac{k_p^2 a_1}{1+\phi_s}\left(g-\frac{\phi_f}{1+\phi_s}\right) = \alpha a'\sin(k'\zeta') + R, \tag{4.8}$$

and for $\perp=2$ it is approximately

$$\frac{k_p^2 a_2}{1+\phi_s}\left(g-\frac{\phi_f}{1+\phi_s}\right) = 0, \tag{4.9}$$

where in Eq. (4.8) the term $\alpha a'\sin(k'\zeta')$ comes from $a_1 \approx a\sin(k\zeta)$ times the $\cos\theta_\pm$ terms in Eq. (4.7) and

$$\alpha = \frac{k_p^4 a^2}{4\sqrt{2}(1+a^2/2)^2}\left(\frac{1}{k_+^2}+\frac{1}{k_-^2}\right), \tag{4.10}$$

$$\begin{aligned}R =\ & A\sin(k\zeta) + B\sin(3k\zeta) + C\sin(2k\zeta + k'\zeta')\\ &+ D\sin(2k\zeta - k'\zeta').\end{aligned} \tag{4.11}$$

The 3-ω term $\sin(3k\zeta)$ is the source of third-harmonic generation [20]. It was shown in our previous works that for the three-dimensional case R also contains 2-ω terms $\sin(2k\zeta)$ and $\cos(2k\zeta)$ which are the source of second-harmonic generation [20], and the slowly varying 0-ω term which is the source of terahertz radiation [21]. In this paper we are concerned with only the 1-ω term $\alpha a'\sin(k'\zeta')$, which changes the refractive index η' for the probe beam. From Eqs. (4.6), (4.8), and (4.9), in the $\hat{x}$ direction ($\perp=1$) the probe beam satisfies

$$\left(\nabla^2 - \frac{1}{c^2}\frac{\partial^2}{\partial t^2} - \frac{k_p^2}{1+\phi_s}\right)\frac{a'}{\sqrt{2}}\sin(k'\zeta') = \alpha a'\sin(k'\zeta'), \tag{4.12}$$

and in the $\hat{y}$ direction ($\perp=2$)

$$\left(\nabla^2 - \frac{1}{c^2}\frac{\partial^2}{\partial t^2} - \frac{k_p^2}{1+\phi_s}\right)\frac{a'}{\sqrt{2}}\sin(k'\zeta') = 0. \tag{4.13}$$

Since

$$\sin(k'\zeta') = -\frac{1}{k'^2c^2}\frac{\partial^2}{\partial t^2}\sin(k'\zeta'), \tag{4.14}$$

Eqs. (4.12) and (4.13) can be written respectively as

$$\left(\nabla^2 - \frac{\eta_x'^2}{c^2}\frac{\partial^2}{\partial t^2}\right)a'\sin(k'\zeta') = 0, \tag{4.15}$$

$$\left(\nabla^2 - \frac{\eta_y'^2}{c^2}\frac{\partial^2}{\partial t^2}\right)a'\sin(k'\zeta') = 0, \tag{4.16}$$

where

$$\eta_x' = \sqrt{1 - \frac{k_p^2/k'^2}{1+\phi_s} - \frac{\sqrt{2}\alpha}{k'^2}}, \tag{4.17}$$

$$\eta_y' = \sqrt{1 - \frac{k_p^2/k'^2}{1+\phi_s}}. \tag{4.18}$$

The birefringence effect represented by $\eta_y' - \eta_x'$ is

$$\eta_y' - \eta_x' \approx \frac{\sqrt{2}\alpha}{2k'^2} = \frac{k_p^4 a^2}{8(1+a^2/2)^2 k'^2}\left(\frac{1}{k_+^2} + \frac{1}{k_-^2}\right). \tag{4.19}$$

The intensity scaling is $\eta_y' - \eta_x' \propto a^2/(1+a^2/2)^2$, the density scaling is $\eta_y' - \eta_x' \propto k_p^4 \propto n_0^2$, and the wave number dependence is $\eta_y' - \eta_x' \propto (1/k'^2)(1/k_-^2 + 1/k_+^2)$, where $k_\pm = k \pm k'$. Equation (4.19) is verified by particle-in-cell simulation in Sec. V.

An intuitive way of understanding the origin of this relativistic birefringence is by looking at the Maxwell equation of Eq. (4.2). In Eq. (4.2), the right-hand side is proportional to $n_e\beta_\perp$, which represents the "nonlinear current density" resulting from the nonlinear motion of the electrons. It can be decomposed into two terms as shown in Eq. (4.3). The first term $a_\perp/(1+\phi_s)$ is isotropic in the x-y polarization plane, which yields the isotropic refractive indices shown in Eq. (4.5). The second term, as shown in the right-hand side of Eq. (4.6), contains a plasma wave of the form $\cos(k\zeta \pm k'\zeta')$ multiplied by $a_\perp$. To the lowest order this term represents the scattering of the pump beam into the probe beam by the plasma wave. Because the pump beam is polarized along the x axis, the scattered wave adds to the probe beam only in the x axis direction. This scattered wave modifies the refractive index along the x axis. The plasma wave of the form $\cos(k\zeta \pm k'\zeta')$ can be traced back to the nonlinear interaction $(\mathbf{v}/c) \times \mathbf{B}$ in the Lorentz force. This nonlinear interaction is significant only in the relativistic regime, where $|\mathbf{v}/c|$ is not much smaller than 1. The mixing of the pump and the probe beams by the $(\mathbf{v}/c) \times \mathbf{B}$ term results in a modulation of the form $\cos(k\zeta \pm k'\zeta')$ in the electron motion, which in turn yields an electron density modulation (plasma wave) of the same form through the continuity equation.

V. COMPARISON WITH PARTICLE-IN-CELL SIMULATIONS

In this section the theoretical result given in Eq. (4.19) is examined by one-dimensional particle-in-cell simulation [35]. In the simulations, a linearly polarized pump pulse with a fixed wavelength $\lambda = 810$ nm and a linearly polarized probe pulse with various wavelengths λ' copropagate in a plasma slab of length L. The probe pulse is 45° polarized with respect to the polarization axis of the pump pulse. The wavelength of the probe pulse is chosen to be far enough from that of the pump pulse such that the self-phase-modulation or Raman scattering of the pump pulse does not interfere with the birefringent effect. The full width at half maximum (FWHM) pulse durations of the pump pulse and the probe pulse are 162 and 49 fs, respectively. The duration of the pump pulse is chosen to be short enough such that for the range of a in the simulations the pulse energy is within the reach of a tabletop multiterawatt laser. It is also chosen to be long enough compared with the period of plasma oscillation to reduce transient effects. The duration of the probe pulse is chosen to be smaller than that of the pump pulse such that it samples the peak region of the pump pulse. It is also chosen to be long enough such that the effect of group velocity dispersion is negligible. The total length of the simulation domain is 230 μm and the grid size is $\Delta z = \lambda'/1024$. The simulation is carried out in the moving-window mode to save computation time and memory usage. A 22-μm-long density ramp is placed at the plasma-vacuum interface to reduce the transition effects induced by the laser pulses while entering the plasma slab. In order to determine the phase of the probe pulse precisely, the simulated wave form of the probe pulse is curve fitted to a sine wave at the pulse peak. This enables accurate calculation of the phase difference between the two orthogonal polarizations in the probe pulse.

From Eq. (4.19), it is seen that the optical path difference $\delta_L = (\eta_y' - \eta_x')L$ satisfies

$$F(\delta_L) \equiv \frac{8k'^2\delta_L}{k_p^4 L}\left(\frac{1}{k_+^2} + \frac{1}{k_-^2}\right)^{-1} = \frac{a^2}{(1+a^2/2)^2}. \tag{5.1}$$

In the simulation we measure the difference of the location $\delta_L = z_{x_{\max}} - z_{y_{\max}}$, where $z_{x_{\max}}$ and $z_{y_{\max}}$ are the points at which the $\hat{x}$- and $\hat{y}$-direction fields have the maximum value. We compare the data $F(\delta_L) = [(8k'^2\delta_L)/(k_p^4 L)](1/k_+^2 + 1/k_-^2)^{-1}$ with the theoretical result $F(\delta_L) = a^2/(1+a^2/2)^2$ in Fig. 1, where $\lambda' = 2\pi/k'$ ranges between 472 and 574 nm, $n_0 = m_e c^2 k_p^2/(4\pi e^2)$ ranges between $6.7 \times 10^{18}/\text{cm}^3$ and $2.8 \times 10^{19}/\text{cm}^3$, and L ranges between 383 and 880 μm.

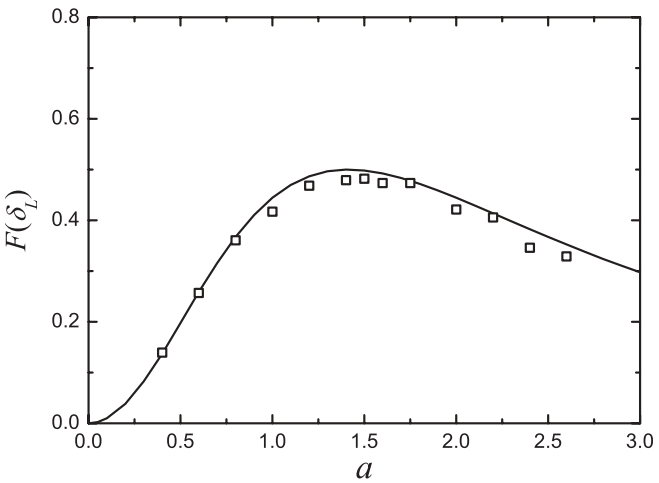

FIG. 1. Comparison between the simulation data (squares) and the theoretical prediction (curve) given in Eq. (5.1). The label for the x axis is the amplitude a of the normalized vector potential defined by Eq. (2.1), and the label for the y axis is the function of the optical path difference $F(\delta_L)$ defined by Eq. (5.1). Both of them are dimensionless quantities. For the data with ascending a, the wavelength of the probe pulse, the plasma density, and the propagation distance are λ' (nm) = 475, 472, 492, 512, 533, 554, 475, 574, 532, 475, 477, 482, and 502, n_0 ($10^{18}/\text{cm}^3$) = 20, 28, 18, 13, 10, 8, 10, 6.7, 7, 7, 8, 7.5, and 7, and L (μm) = 582, 383, 383, 383, 383, 383, 482, 383, 582, 880, 781, 781, and 781, respectively.

All the simulation data fall close to the theoretical curve of Eq. (5.1) and thus support the theory well.

VI. DISCUSSION AND SUMMARY

The phase difference between the two orthogonal polarizations of the probe pulse $\Delta\phi = k'(\eta'_y - \eta'_x)L$ is on the order of 10^{-2} for the ranges of a, n_0, k, k', L considered in this paper. Although this is a small phase difference, it can be measured by using the technique of balanced detection, which has a typical phase sensitivity of 10^{-4} [36]. To reach the condition of $L \approx 400\ \mu$m, the pump pulse must be focused to a spot size for which the confocal parameter is larger than 200 μm. This means the FWHM focal spot size must be larger than 8.5 μm. In the meantime, to reach the condition of $a = 2$, the intensity of the pump laser at the focal spot must exceed 8.4×10^{18} W/cm^2 for $\lambda = 810$ nm. These two conditions imply that the pump laser must be able to deliver 1.2 J of energy if the pulse duration is set to be $\approx$160 fs and proportionally for other pulse durations. This condition can be met by existing tabletop high-power lasers based on chirped-pulse amplification.

In designing an experiment with a realistic three-dimensional laser beam, one should keep the plasma density low enough to avoid transverse modulational instability. From the nonlinear refractive index in Eqs. (3.12) and (4.5) and the analysis in Ref. [12], transverse modulational instability becomes a concern when

$$\frac{w_0^2\omega_p^2}{8c^2}\left(1 - \frac{1}{\sqrt{1+a^2/2}}\right) > 1. \tag{6.1}$$

Therefore the constraint on plasma density set by the transverse modulational instability is

$$n_0 < \frac{8c^2 m_e}{4\pi e^2 w_0^2 (1 - 1/\sqrt{1+a^2/2})}. \tag{6.2}$$

All the cases of particle-in-cell simulation presented in Fig. 1 satisfy this constraint. For the laser parameters we suggested $a = 1$–2, $w_0 = 7.2\ \mu$m (FWHM focal spot size of 8.5 μm), and the density should be kept below $(2.4\text{–}1.0)\times 10^{19}$ cm^{-3}.

In Sec. V we limited our discussion to the case of $|k - k'| = O(k)$. Such a consideration arises from the experimental point of view. If k' is close to k, the pump pulse may generate frequency components at the frequency of the probe pulse by self-phase-modulation and Raman scattering. These frequency components will interfere with the birefringence measurement. From a theoretical point of view the case of $k' \to k$ can also be analyzed by the same method. The only difference between these two cases is in the proper separation of the fast and slow components in the nonlinear source terms. When $k' \to k$, from Eq. (3.1) one has $\eta' \to \eta$ and $k'\zeta' \to k\zeta$; hence the term $\cos\theta_- = \cos(k\zeta - k'\zeta')$ approaches 1. For this case the term $\cos\theta_-$ should not be included in the fast-oscillating part of $\gamma/(1+\phi) - 1$ [the right-hand side of Eq. (3.9)] and hence should disappear in ϕ_f. Similarly, since the derivative of $\cos\theta_-$ approaches zero, it should also disappear in $df_\parallel/dt$ [the right-hand side of Eq. (3.17)] and $f_\parallel$, and hence in g which contains $f_\parallel$ and $\gamma/(1+\phi) - 1$. For this case Eq. (4.7) then becomes

$$\frac{k_p^2}{1+\phi_s}\left(g - \frac{\phi_f}{1+\phi_s}\right) = \frac{k_p^4 aa'}{2\sqrt{2}(1+a^2/2)^2}\left[\frac{3a\cos(2k\zeta)}{4\sqrt{2}a'k^2} + \left(\frac{1}{kk'} - \frac{1}{k_+^2}\right)\cos\theta_+\right]. \tag{6.3}$$

Multiplying Eq. (6.3) by $a_1 \approx a\sin(k\zeta)$, one obtains that for the case $k' \to k$

$$\alpha = \frac{-k_p^4 a^2}{4\sqrt{2}(1+a^2/2)^2}\left(\frac{1}{kk'} - \frac{1}{k_+^2}\right), \tag{6.4}$$

and Eq. (4.19) becomes

$$\eta'_y - \eta'_x \approx \frac{\sqrt{2}\alpha}{2k'^2} = \frac{-k_p^4 a^2}{8(1+a^2/2)^2 k'^2}\left(\frac{1}{kk'} - \frac{1}{k_+^2}\right), \tag{6.5}$$

where $k_+ = k + k'$. Namely, for the case $k' \to k$, one has

$$\eta'_y - \eta'_x \approx \frac{-3k_p^4 a^2}{32(1+a^2/2)^2 k^4}. \tag{6.6}$$

In summary, we analyzed the effect of relativistic birefringence induced by a high-intensity laser field in plasma. The phase difference for the parallel and perpendicular polarizations caused by the relativistic motion of electrons is proportional to the square of the plasma density, and its dependence on intensity reaches a maximum at $a = \sqrt{2}$. The saturation at $a > \sqrt{2}$ is due to the relativistic mass increase of electrons. The analytical result was compared with particle-in-cell simulations, and the agreement provides good support for the theory. For typical intensities, densities, and interaction lengths in experiments in high-field physics, the phase difference is well above the detection threshold. This nonlinear effect may thus be utilized for the diagnosis of relativistic laser-plasma interactions or characterization of laser pulses with relativistic intensity, for which conventional nonlinear optics is impeded by optical breakdown and spectral limitation.

ACKNOWLEDGMENTS

The work was supported by the National Science Council under Contracts No. NSC 98-2115-M-029-003 and No. NSC 98-2112-M-001-013-MY3. The authors would like to acknowledge the National Center for High-Performance Computing, Taiwan for providing resources under the national project "Taiwan Knowledge Innovation National Grid," and the National Center for Theoretical Sciences, Taiwan for general financial support.

[1] G. A. Mourou, T. Tajima, and S. V. Bulanov, Rev. Mod. Phys. **78**, 309 (2006).

[2] S. Y. Chen, A. Maksimchuk, E. Esarey, and D. Umstadter, Phys. Rev. Lett. **84**, 5528 (2000).

[3] E. Takahashi, M. Mori, N. Yugami, Y. Nishida, and K. Kondo, Phys. Rev. E **65**, 016402 (2001).

[4] C. C. Kuo, C. H. Pai, M. W. Lin, K. H. Lee, J. Y. Lin, J. Wang, and S. Y. Chen, Phys. Rev. Lett. **98**, 033901 (2007).

[5] P. Monot, T. Auguste, P. Gibbon, F. Jakober, G. Mainfray, A. Dulieu, M. Louis-Jacquet, G. Malka, and J. L. Miquel, Phys. Rev. Lett. **74**, 2953 (1995).
[6] V. Malka, J. Faure, J. R. Marques, F. Amiranoff, C. Courtois, Z. Najmudin, K. Krushenick, M. R. Salvati, and A. E. Dangor, IEEE Trans. Plasma Sci. **28**, 1078 (2000).
[7] J. Faure, V. Malka, J. R. Marques, P. G. David, F. Amiranoff, K. T. Phuoc, and A. Rousse, Phys. Plasmas **9**, 756 (2002).
[8] Z. Najmudin *et al.*, IEEE Trans. Plasma Sci. **28**, 1057 (2000).
[9] J. Faure, Y. Glinec, J. J. Santos, F. Ewald, J. P. Rousseau, S. Kiselev, A. Pukhov, T. Hosokai, and V. Malka, Phys. Rev. Lett. **95**, 205003 (2005).
[10] H. Hamster, A. Sullivan, S. Gordon, W. White, and R. W. Falcone, Phys. Rev. Lett. **71**, 2725 (1993).
[11] W. P. Leemans *et al.*, Phys. Rev. Lett. **91**, 074802 (2003).
[12] W. B. Mori, IEEE J. Quantum Electron. **33**, 1942 (1997).
[13] P. R. Bolton and B. Ritchie, J. Opt. Soc. Am. B **14**, 437 (1997).
[14] P. Sprangle, C. Tang, and E. Esarey, IEEE Trans. Plasma Sci. **PS-15**, 145 (1987).
[15] P. Sprangle, E. Esarey, and A. Ting, Phys. Rev. A **41**, 4463 (1990).
[16] B. Hafizi, A. Ting, P. Sprangle, and R. F. Hubbard, Phys. Rev. E **62**, 4120 (2000).
[17] J. Penano, P. Sprangle, B. Hafizi, D. Gordon, and P. Serafim, Phys. Rev. E **81**, 026407 (2010).
[18] N. Naseri, S. G. Bochkarev, and W. Rozmus, Phys. Plasmas **17**, 033107 (2010).
[19] J. M. Rax and N. J. Fisch, Phys. Rev. Lett. **69**, 772 (1992).
[20] G. Y. Tsaur and J. Wang, Phys. Rev. A **76**, 063815 (2007).
[21] G. Y. Tsaur and J. Wang, Phys. Rev. A **80**, 023802 (2009).
[22] P. Chessa, P. Mora, and T. M. Antonsen Jr., Phys. Plasmas **5**, 3451 (1998).
[23] M. Lontano and I. G. Murusidze, Opt. Express **11**, 248 (2003).
[24] N. M. Naumova, S. V. Bulanov, K. Nishihara, T. Z. Esirkepov, and F. Pegoraro, Phys. Rev. E **65**, 045402(R) (2002).
[25] L. Cao, W. Yu, H. Xu, C. Zheng, Z. Liu, B. Li, and A. Bogaerts, Phys. Rev. E **70**, 046408 (2004).
[26] Z. M. Sheng, H. C. Wu, K. Li, and J. Zhang, Phys. Rev. E **69**, 025401(R) (2004).
[27] Z. M. Sheng, K. Mima, J. Zhang, and H. Sanuki, Phys. Rev. Lett. **94**, 095003 (2005).
[28] D. Dahiya, V. Sajal, and A. K. Sharma, Phys. Plasmas **14**, 123104 (2007).
[29] M. E. Fermann, L. M. Yang, M. L. Stock, and M. J. Andrejco, Opt. Lett. **19**, 43 (1994).
[30] C. K. Nielsen and S. R. Keiding, Opt. Lett. **32**, 1474 (2007).
[31] R. Trebino and D. J. Kane, J. Opt. Soc. Am. A **10**, 1101 (1993).
[32] A. Jullien *et al.*, Opt. Lett. **30**, 920 (2005).
[33] M. Fujimoto, S. Aoshima, M. hosoda, and Y. Tsuchia, Opt. Lett. **24**, 850 (1999).
[34] T. Heinzl, B. Liesfeld, K. Amthor, H. Schwoerer, R. Sauerbrey, and A. Wipf, Opt. Commun. **267**, 318 (2006).
[35] C. Nieter and J. R. Cary, J. Comput. Phys. **196**, 488 (2004).
[36] Philip C. D. Hobbs, *Building Electro-Optical Systems: Making It All Work*, (John Wiley & Sons, New York, 2000), Sec. 18.5.

Relativistic birefringence induced by high-intensity laser field in plasma

G. Tsaur[1], N.-H. Kang[2], Z.-H. Xie[3], S.-H. Chen[4], J. Wang[3,4,5]

[1]*Department of Mathematics, Tunghai University, Taichung 40704, Taiwan*
[2]*Department of Physics, National Tsing Hua University, Hsinchu 30013, Taiwan*
[3]*Department of Physics, National Taiwan University, Taipei 10617, Taiwan*
[4]*Department of Physics, National Central University, Jhongli 32001, Taiwan*
[5]*Institute of Atomic and Molecular Sciences, Academia Sinica, Taipei 10617, Taiwan*

gytsaur@thu.edu.tw

Abstract: An analytical expression for relativistic birefringence induced by high-intensity laser field in plasma is derived. Its dependence on intensity, wavelength, and density is clearly displayed. The theory is verified by particle-in-cell simulation.

OCIS codes: 350.5400 (Plasmas), 350.5720 (Relativity).

1. Introduction

Field-induced birefringence, also known as cross-polarization wave generation, has played an important role in ultrafast nonlinear optics. It is utilized to achieve passive mode-locking in fiber lasers [1, 2] as well as to enhance the contrast of high-intensity lasers [3]. It is also the key element of frequency-resolved-optical-gating for femtosecond waveform characterization [4].

In this paper we study relativistic birefringence induced by a strong propagating laser field in underdense plasmas. For relativistic nonlinear optics it is natural to consider a fully ionized plasma as the nonlinear medium. This is because plasma will not be damaged by high-intensity laser, and plasma is not limited by absorption in the deep UV spectral range and beyond. In addition, transient plasma structures can be fabricated by synchronized laser pulses to enhance the nonlinear interaction [5]. We analyze the relativistic motion of plasma electrons driven by a strong linearly-polarized pump beam and a weak probe beam polarized at 45° with respect to the polarization axis of the pump beam. Because of the nonlinear relativistic motion of the electrons, the probe beam experiences different indexes of refraction in its two polarization axes as a function of the intensity of the pump beam, the plasma density, and the wavelengths of the pump and probe beams. The induced birefringence rotates the polarization of the probe beam.

In relativistic nonlinear optics, a relevant parameter is the amplitude a of the normalized vector potential. Relativistic effects become significant when a is not much smaller than 1. Although relativistic nonlinear effects can be analyzed by using a as the perturbation parameter, such an approach is valid only when $a \ll 1$. This is too restrictive considering that currently a tabletop multi-terawatt laser can easily produce a field of $a > 1$. In this paper we use a'/a and $1-\eta^2$ as the perturbation parameters to derive the first-order analytical solution that describes the relativistic birefringence induced by a laser beam, where a, a' are the amplitudes of the pump beam and probe beam respectively, and η is the index of refraction. The starting point (unperturbed solution) is the fully relativistic solution for the case with $a' = 0$ and $\eta = 1$, which is exact for arbitrary a [6]. For most experiments $1-\eta^2$ is on the order of 10^{-2} and a'/a can be chosen $\ll 1$, hence the first-order terms in the expansion already provide a useful approximate solution without being limited to $a \ll 1$.

2. Solutions for the relativistic electron motion

The normalized vector potential $\mathbf{a} = a_1\hat{x} + a_2\hat{y} + a_3\hat{z}$ of the pump and probe combined laser field is $a_1 = a\sin(k\zeta) + a'\sin(k'\zeta')/\sqrt{2}$, $a_2 = a'\sin(k'\zeta')/\sqrt{2}$, and $a_3 = 0$, where $\zeta = \eta z - ct$, $\zeta' = \eta' z - ct$, and η, η' are the refractive index of the pump and probe beams respectively. The Lorentz equation is given by

$$\frac{d\mathbf{p}}{dt} = m_e c^2 \left[\frac{1}{c}\frac{\partial \mathbf{a}}{\partial t} + \nabla\phi - \boldsymbol{\beta} \times (\nabla \times \mathbf{a})\right], \tag{1}$$

$$\frac{d}{dt}(m_e c\gamma) = m_e c^2 \boldsymbol{\beta} \cdot \left(\frac{1}{c}\frac{\partial \mathbf{a}}{\partial t} + \nabla\phi\right), \tag{2}$$

where $\beta = \mathbf{v}/c$. The normalized scalar potential ϕ in Eqs. (1) and (2) satisfies the Poisson equation

$$\nabla^2\phi = k_p^2(n_e/n_0 - 1), \tag{3}$$

where $k_p = \omega_p/c$ and ω_p is the plasma frequency. The quantities n_e and β in Eqs. (1) and (2) are related by the continuity equation

$$\partial n_e/\partial t + c\nabla\cdot(n_e\beta) = 0. \tag{4}$$

The solutions are $\mathbf{p} = m_e c\gamma\beta$ and

$$\beta_\perp = \frac{a_\perp}{\gamma}, \quad \beta_\parallel = \eta - \frac{\eta(1+\phi-f_\parallel)}{\gamma}, \tag{5}$$

$$\gamma = \frac{1+a_\perp^2+\eta^2(1+\phi-f_\parallel)^2}{2\eta^2(1+\phi-f_\parallel)} - (1-\eta^2)\frac{[1+a_\perp^2+\eta^2(1+\phi-f_\parallel)^2]^2}{8\eta^6(1+\phi-f_\parallel)^3}, \tag{6}$$

where the subscript $\perp$ represents the x and y components and the subscript $\parallel$ represents the z component. Under the condition $|k-k'| = O(k)$ the solutions of $\phi = \phi_s + \phi_f$, $f_\parallel$, and n_e are

$$\phi_s = \sqrt{1+\frac{a^2}{2}} - 1, \quad \phi_f = \frac{k_p^2}{2(1+a^2/2)}\left[\frac{a^2}{8k^2}\cos(2k\zeta) + \frac{aa'}{\sqrt{2}}\left(\frac{\cos\theta_+}{k_+^2} - \frac{\cos\theta_-}{k_-^2}\right)\right], \tag{7}$$

$$f_\parallel = \frac{k_p^2 aa'}{4\sqrt{2}(1+a^2/2)k^2k'}\left(k_-\cos\theta_+ + k_+\cos\theta_-\right), \tag{8}$$

$$\frac{n_e}{n_0} = \frac{\gamma}{1+\phi}\left\{1 + \frac{k_p^2}{2(1+a^2/2)^{3/2}}\left[\frac{a^2}{2k^2}\cos(2k\zeta) + \frac{aa'}{\sqrt{2}kk'}\left(\cos\theta_+ + \cos\theta_-\right)\right]\right\}, \tag{9}$$

where $\theta_\pm \equiv k\zeta \pm k'\zeta'$ and $k_\pm \equiv k \pm k' = O(k)$.

3. Relativistic birefringence

The time dependent electron density n_e, electron velocity β, and the potential function ϕ serve as the source terms of the Maxwell equation, from which the change of the refractive indexes in the two perpendicular axes can be derived. In the Coulomb gauge $\nabla\cdot\mathbf{a} = 0$, the normalized transverse Maxwell equation is

$$\left(\nabla^2 - \frac{1}{c^2}\frac{\partial^2}{\partial t^2}\right)a_\perp = k_p^2\frac{n_e}{n_0}\beta_\perp. \tag{10}$$

From the solutions given in Eqs. (5)–(9) one can evaluate the right hand side of Eq. (10) and show that the probe beam satisfies in the $\hat{x}$ direction ($\perp = 1$)

$$\left(\nabla^2 - \frac{\eta_x'^2}{c^2}\frac{\partial^2}{\partial t^2}\right)a'\sin(k'\zeta') = 0, \tag{11}$$

and in the $\hat{y}$ direction ($\perp = 2$)

$$\left(\nabla^2 - \frac{\eta_y'^2}{c^2}\frac{\partial^2}{\partial t^2}\right)a'\sin(k'\zeta') = 0, \tag{12}$$

where

$$\eta_y' - \eta_x' \approx \frac{k_p^4 a^2}{8(1+a^2/2)^2k'^2}\left(\frac{1}{k_+^2} + \frac{1}{k_-^2}\right). \tag{13}$$

The intensity scaling is $\eta_y' - \eta_x' \propto a^2/(1+a^2/2)^2$, the density scaling is $\eta_y' - \eta_x' \propto k_p^4 \propto n_0^2$, and the wave number dependence is $\eta_y' - \eta_x' \propto (1/k'^2)(1/k_-^2 + 1/k_+^2)$, where $k_\pm = k \pm k'$. Eq. (13) is verified by particle-in-cell simulation in Section 4.

4. Comparison with particle-in-cell simulations

In the simulations, a linearly-polarized pump pulse with a fixed wavelength λ = 810 nm and a linearly-polarized probe pulse with various wavelength λ' are set to co-propagate in a plasma slab of length L. The probe pulse is 45° polarized with respect to the polarization axis of the pump pulse. The wavelength of the probe pulse is chosen to be far enough from that of the pump pulse, such that the birefringent effect is not interfered by the self-phase modulation or Raman scattering of the pump pulse. The full-width-at-half-maximum (FWHM) pulse durations of the pump pulse and the probe pulse are 162 fs and 49 fs respectively. The duration of the pump pulse is chosen to be short enough such that for the range of a in the simulations the pulse energy is within the reach of a tabletop multi-terawatt laser. It is also chosen to be long enough comparing with the period of plasma oscillation to reduce transient effects. The duration of the probe pulse is chosen to be smaller than that of the pump pulse such that it samples the peak region of the pump pulse. It is also chosen to be long enough such that the effect of group velocity dispersion is negligible. The total length of the simulation domain is 230 μm and the grid size is $\Delta z = \lambda'/1024$. The simulation is carried out in the moving-window mode to save computation and memory usage. A 22-μm long density ramp is placed at the plasma-vacuum interface to reduce the transition effects induced by the laser pulses while entering the plasma slab. In order to determine the phase of the probe pulse precisely, the simulated waveform of the probe pulse is curve fitted to a sine wave at the pulse peak. This enables accurate calculation of the phase difference between the two orthogonal polarizations in the probe pule. By calculating the optical path difference $\delta_L = (\eta'_y - \eta'_x)L$ from the simulation data, we plot the function $F(\delta_L) = (8k'^2\delta_L)/(k_p^4 L)\left(1/k_+^2 + 1/k_-^2\right)^{-1}$ and compare it with the theoretical result $F(\delta_L) = a^2/(1+a^2/2)^2$ in Fig. 1. All the simulation data fall close to the theoretical curve of Eq. (13) and thus support the theory well.

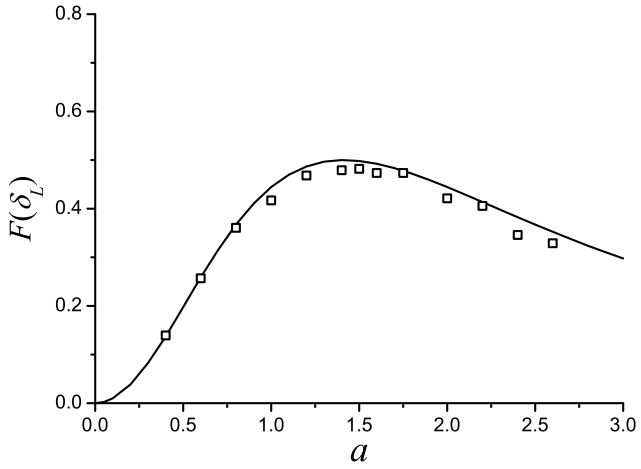

Fig. 1. Comparison between the simulation data (square) and the theoretical prediction (curve) given in Eq. (13). For the data with ascending a, the wavelength of the probe pulse, the plasma density, and the propagation distance are λ'(nm) = 475, 472, 492, 512, 533, 554, 475, 574, 532, 475, 477, 482, 502, $n_0(10^{18}/\mathrm{cm}^3)$ = 20, 28, 18, 13, 10, 8, 10, 6.7, 7, 7, 8, 7.5, 7, and $L(\mu\mathrm{m})$ = 582, 383, 383, 383, 383, 383, 482, 383, 582, 880, 781, 781, 781 respectively.

References

1. M. E. Fermann, L. M. Yang, M. L. Stock, and M. J. Andrejco, Opt. Lett. **19**, 43 (1994).
2. C. K. Nielsen and S. R. Keiding, Opt. Lett. **32**, 1474 (2007).
3. A. Jullien et al. Opt. Lett. **30**, 920 (2005).
4. R. Trebino and D. J. Kane, J. Opt. Soc. Am. A, **10**, 1101 (1993).
5. C. C. Kuo et al. Phys. Rev. Lett. **98**, 033901 (2007).
6. P. Sprangle, E. Esarey, and A. Ting, Phys. Rev. A **41**, 4463 (1990).

國科會補助計畫衍生研發成果推廣資料表

日期:2011/10/06

國科會補助計畫	計畫名稱: 由強場雷射所驅動的相對論性電子運動（IV）
	計畫主持人: 曹景懿
	計畫編號: 99-2115-M-029-002- 學門領域: 微分方程

無研發成果推廣資料

99 年度專題研究計畫研究成果彙整表

計畫主持人：曹景懿	計畫編號：99-2115-M-029-002-
計畫名稱：由強場雷射所驅動的相對論性電子運動（IV）	

成果項目			量化			單位	備註（質化說明：如數個計畫共同成果、成果列為該期刊之封面故事...等）
			實際已達成數（被接受或已發表）	預期總達成數(含實際已達成數)	本計畫實際貢獻百分比		
國內	論文著作	期刊論文	0	0	100%	篇	
		研究報告/技術報告	1	1	100%		
		研討會論文	0	0	100%		
		專書	0	0	100%		
	專利	申請中件數	0	0	100%	件	
		已獲得件數	0	0	100%		
	技術移轉	件數	0	0	100%	件	
		權利金	0	0	100%	千元	
	參與計畫人力（本國籍）	碩士生	1	1	100%	人次	
		博士生	0	0	100%		
		博士後研究員	0	0	100%		
		專任助理	0	0	100%		
國外	論文著作	期刊論文	1	1	100%	篇	
		研究報告/技術報告	0	0	100%		
		研討會論文	1	1	100%		
		專書	0	0	100%	章/本	
	專利	申請中件數	0	0	100%	件	
		已獲得件數	0	0	100%		
	技術移轉	件數	0	0	100%	件	
		權利金	0	0	100%	千元	
	參與計畫人力（外國籍）	碩士生	0	0	100%	人次	
		博士生	0	0	100%		
		博士後研究員	0	0	100%		
		專任助理	0	0	100%		

其他成果 (無法以量化表達之成果如辦理學術活動、獲得獎項、重要國際合作、研究成果國際影響力及其他協助產業技術發展之具體效益事項等，請以文字敘述填列。)	無

	成果項目	量化	名稱或內容性質簡述
科教處計畫加填項目	測驗工具(含質性與量性)	0	
	課程/模組	0	
	電腦及網路系統或工具	0	
	教材	0	
	舉辦之活動/競賽	0	
	研討會/工作坊	0	
	電子報、網站	0	
	計畫成果推廣之參與（閱聽）人數	0	

國科會補助專題研究計畫成果報告自評表

請就研究內容與原計畫相符程度、達成預期目標情況、研究成果之學術或應用價值（簡要敘述成果所代表之意義、價值、影響或進一步發展之可能性）、是否適合在學術期刊發表或申請專利、主要發現或其他有關價值等，作一綜合評估。

1. 請就研究內容與原計畫相符程度、達成預期目標情況作一綜合評估

■達成目標

□未達成目標（請說明，以 100 字為限）

□實驗失敗

□因故實驗中斷

□其他原因

說明：

2. 研究成果在學術期刊發表或申請專利等情形：

論文：■已發表 □未發表之文稿 □撰寫中 □無

專利：□已獲得 □申請中 ■無

技轉：□已技轉 □洽談中 ■無

其他：(以 100 字為限)

3. 請依學術成就、技術創新、社會影響等方面，評估研究成果之學術或應用價值（簡要敘述成果所代表之意義、價值、影響或進一步發展之可能性）(以 500 字為限)

在超快非線性光學中，雷射場導致的雙折射現象扮演了很重要的角色。在光纖鎖模雷射中它被用來產生飛秒雷射脈衝；在飛秒雷射波形的測量上，它也是 Frequency-Resolved Optical Gating 的基礎； 在飛秒雷射放大器上它被用來大幅加強雷射脈衝的對比，是目前最有效的方法。傳統的非線性光學是以非線性晶體為介質，不但在光的強度上受到光學損壞的限制，工作的頻率範圍也被吸收波段限制。以電漿為非線性介質可以突破這些限制，因此發展電漿非線性光學是一個重要的課題。在這篇論文中，我們從電子的相對論性運動出發，證明了強場雷射可在電漿中引致相對論性雙折射，並導出它與電漿密度，雷射強度，以及與雷射場和測試場波長的相關性。這個理論已經透過電腦模擬獲得驗證。